

CO₂ Reduction Reaction to Create CH₄ and CH₃OH on Chromium Doped Silicon, Carbon and Boron Nitride (2Cr-Si₇₆, 2Cr-C₇₆ and 2Cr-B₃₈N₃₈)

¹Huaying Gao, ²Xinxin Li*, ³Chun Xiang

¹Library and Information Center of Weifang Engineering Vocational College, Weifang, Shandong, 262500, China.

²College of A&F Science and Technology, Weifang Engineering Vocational College, Weifang, Shandong, 262500, China.

³Shaoxing Hanli Industrial Automation, Shaoxing, Zhejiang, China. 19228641905@163.com*

(Received on 30th April 2025, accepted in revised form 24th December 2025)

Abstract: Here, the pathways for CO₂ reduction reaction to create CH₄ and CH₃OH on Si₇₆, C₇₆ and B₃₈N₃₈ as catalysts are investigated. The effects of adsorption of Cr on capacities of Si₇₆, C₇₆ and B₃₈N₃₈ for CO₂-RR are examined. Results shown that the over-potential of CO₂-RR on 2Cr-Si₇₆, 2Cr-C₇₆ and 2Cr-B₃₈N₃₈ are lower than Fe, Ni and Co single atom as catalysts, Cu, Au, Ag based bimetallic catalysts and Pt and Pd as metal catalysts in previous works. The ΔG_{reaction} of possible reaction steps of CO₂ reduction on 2Cr-Si₇₆ and 2Cr-B₃₈N₃₈ nanocages are more negative than 2Cr-C₇₆ nanocage. The over-potential for production of CH₄ and CH₃OH are lower than creation of HCOOH and HCHO on 2Cr-Si₇₆, 2Cr-C₇₆ and 2Cr-B₃₈N₃₈ nanocages. The over-potential for CO, HCOOH, HCHO, CH₃OH and CH₄ production on 2Cr-B₃₈N₃₈ nanocage is 0.34, 0.27, 0.31, 0.24 and 0.22 V. The 2Cr-Si₇₆ and 2Cr-B₃₈N₃₈ are catalyzed the reaction steps of CO₂-RR by three pathways and high performance.

Keyword: Nano-catalysts, CH₃OH, CO₂-RR, CH₄, reduction reaction mechanism, Metal adsorption.

Introduction

The carbon dioxide (CO₂) has been produced from fossil fuels [1] and CO₂ are one of the main reasons for earth warming [2]. The decreasing and removing the CO₂ has high important to reduce the earth warming [3-5]. The CO₂ can be removed in important reactions and CO₂ can be converted to other species with high performances [5-8]. The organic chemists have confirmed that the reduction reaction of CO₂ can create the HCOOH and CH₃OH molecules [9-11].

The Si and C nanocages and nanotubes have been proposed the novel pathways to design of stable and active catalysts for important reaction in chemical industry [12-14]. The capacities of metals doped Si and C nanocages and nanotubes to catalyze the important organic reactions in chemical industry have been examined [15-17]. Researchers shown than the Si, BN and C nanocages and nanotubes have effective properties for CO₂-RR in normal temperature [17]. In recent years, researchers have shown that the metal catalysts due to their high price, low stability, low selectivity and low performances have low efficiency for oxidation and reduction of toxic gases [11-15].

In previous works [11-15] the capacities of various metal catalysts including the Fe, Ni and Co single atom, Cu, Au, Ag based bimetallic and Pt and Pd as

catalysts for CO₂-RR have been examined. The possible pathways for CO₂-RR on various metal catalysts including the Fe, Ni and Co single atom, Cu, Au, Ag based bimetallic and Pt and Pd have been investigated [11-15]. Results have shown that the metal catalysts (Fe, Ni and Co single atom, Cu, Au, Ag based bimetallic and Pt and Pd) have high price and low selectivity for catalyze the reaction steps of CO₂-RR in normal temperature [11-15].

In this work, the pathways for CO₂-RR for formation the CO, CH₄, HCOOH, HCHO and CH₃OH species on 2Cr-Si₇₆, 2Cr-C₇₆ and 2Cr-B₃₈N₃₈ are investigated. The effects of adsorption of Cr atoms of 2Cr-Si₇₆, 2Cr-C₇₆ and 2Cr-B₃₈N₃₈ on their capacities for CO₂-RR are examined. The capacities of 2Cr-Si₇₆, 2Cr-C₇₆ and 2Cr-B₃₈N₃₈ for CO₂-RR are compared. The catalysts and pathways on 2Cr-Si₇₆, 2Cr-C₇₆ and 2Cr-B₃₈N₃₈ for CO₂-RR are proposed with high efficiency. The goals of this work are: to compare the abilities of 2Cr-Si₇₆, 2Cr-C₇₆ and 2Cr-B₃₈N₃₈ of CO₂-RR; to suggest the new catalysts (2Cr-Si₇₆, 2Cr-C₇₆ and 2Cr-B₃₈N₃₈) for CO₂-RR, to compare the catalytic activity of various nanocages for CO₂-RR, to find the effective pathways for CO₂-RR, to compare the efficiency of 2Cr-Si₇₆, 2Cr-C₇₆ and 2Cr-B₃₈N₃₈ for CO₂-RR with metal based catalysts.

*To whom all correspondence should be addressed.

Computational Details

The M06-2X/6-311+G (2d, 2p), PBEPBE/6-311+G (2d, 2p) and B3LYP-D3/6-311+G (2d, 2p) methods have been used to optimize the Si₇₆, C₇₆, B₃₈N₃₈, 2Cr-Si₇₆, 2Cr-C₇₆ and 2Cr-B₃₈N₃₈ nanocages and their complexes with species in GAMESS software [16]. In this study the transition states of reaction step of CO₂-RR on 2Cr-Si₇₆, 2Cr-C₇₆ and 2Cr-B₃₈N₃₈ have been obtained with opt=qst3 and results have shown that there is only one imaginary frequency for transition states of reaction step of CO₂-RR on 2Cr-Si₇₆, 2Cr-C₇₆ and 2Cr-B₃₈N₃₈ [17-19]. In this study the COSMO (Conductor-like screening model) model as an implicit solvation model has been used to consider the effects of solvent (water as polar solvent) on reaction steps of possible mechanisms of CO₂-RR by M06-2X /6-311+G (2d, 2p) method [20].

In this study, the acceptable spin states and spin multiplicities (S = 3, 2 and 1 and 2S+1 = 7, 5 and 3) of Cr atoms in 2Cr-Si₇₆, 2Cr-C₇₆ and 2Cr-B₃₈N₃₈ and complexes of 2Cr-Si₇₆, 2Cr-C₇₆ and 2Cr-B₃₈N₃₈ with intermediates of CO₂-RR have been considered [19, 20]. The complexes of intermediates of CO₂-RR have been optimized and their frequencies have been calculated [20]. The adsorption free Gibbs energies ($\Delta G_{\text{adsorption}}$) of CO₂ and intermediates of CO₂-RR on 2Cr-Si₇₆, 2Cr-C₇₆ and 2Cr-B₃₈N₃₈ are calculated [21]:

$$\Delta G_{\text{adsorption}} = G_{\text{specie-nanocage}} - G_{\text{specie}} - G_{\text{nanocage}} \quad (1)$$

The G_{nanocage} is free Gibbs energies of 2Cr-Si₇₆, 2Cr-C₇₆ and 2Cr-B₃₈N₃₈ nanocages and G_{specie} is free Gibbs energies of intermediates of CO₂ reduction reactions and the $G_{\text{specie-nanocage}}$ is free Gibbs energies of complexes of 2Cr-Si₇₆, 2Cr-C₇₆ and 2Cr-B₃₈N₃₈ nanocages with intermediates of CO₂ reduction reactions [19].

The $\Delta G_{\text{reaction}}$ of reaction steps of CO₂ reduction reactions on 2Cr-Si₇₆, 2Cr-C₇₆ and 2Cr-B₃₈N₃₈ are calculated [20-23]:

$$\Delta G_{\text{reaction}} = \Delta E + \Delta ZPE - T\Delta S + eU + \Delta G_{\text{pH}} \quad (2)$$

The T, E, S and ZPE are temperature, energy, entropy and zero-point energy of complexes of Si₇₆, C₇₆, B₃₈N₃₈, 2Cr-Si₇₆, 2Cr-C₇₆ and 2Cr-B₃₈N₃₈ with species [24]. The ΔG_{pH} as free energy correction because of variations in H⁺ concentration can be calculated by $G_{\text{pH}} = -kT \ln [H^+] = kT \ln 10 \times \text{pH}$, and pH is 0. The U and e are applied potential and number of electron transfer, respectively [24]. The U is potential of electrode commissioned to electrode of standard hydrogen and the values of U is started since 0 until 1.23 V in balance potential U₀ and several stages of CO₂-RR are formidable. The used potential U is requested to eliminate positive part of Gibbs free energy and

overvoltage is defined as $\eta = U_0 - U$ [24, 25]. The zero-point energy and entropy contributions of nanocages (Si₇₆, C₇₆ and B₃₈N₃₈), metal doped nanocages (2Cr-Si₇₆, 2Cr-C₇₆ and 2Cr-B₃₈N₃₈) and their complexes of intermediates of reaction steps of CO₂-RR on 2Cr-Si₇₆, 2Cr-C₇₆ and 2Cr-B₃₈N₃₈ have been calculated by vibrational frequencies of optimized structures by M06-2X /6-311+G (2d, 2p) method [17-20].

Results and Discussion

Nanocages (Si₇₆, C₇₆ and B₃₈N₃₈ and 2Cr-Si₇₆, 2Cr-C₇₆ and 2Cr-B₃₈N₃₈)

The properties of Si₇₆, C₇₆ and B₃₈N₃₈ nanocages and 2Cr-doped structures (2Cr-Si₇₆, 2Cr-C₇₆ and 2Cr-B₃₈N₃₈) are investigated. The Si₇₆, C₇₆, B₃₈N₃₈, 2Cr-Si₇₆, 2Cr-C₇₆ and 2Cr-B₃₈N₃₈ nanocages are presented in Figure 1. The $\Delta G_{\text{adsorption}}$ [25-28] values of Cr on Si₇₆, C₇₆ and B₃₈N₃₈ are examined in Table 1:

$$\Delta G_{\text{adsorption}} = G_{2\text{Cr-nanocage}} - G_{\text{nanocage}} - 2G_{\text{Cr}} \quad (3)$$

The G_{nanocage} is free Gibbs energies of Si₇₆, C₇₆ and B₃₈N₃₈ nanocages and G_{Cr} is free Gibbs energy of Cr and $G_{2\text{Cr-nanocage}}$ is free Gibbs energies of Cr with Si₇₆, C₇₆ and B₃₈N₃₈. The $\Delta G_{\text{adsorption}}$ of 2Cr-Si₇₆, 2Cr-C₇₆ and 2Cr-B₃₈N₃₈ nanocages are -6.79, -6.21 and -6.46 eV. The 2Cr-Si₇₆ and 2Cr-B₃₈N₃₈ nanocages have higher $\Delta G_{\text{adsorption}}$ than 2Cr-C₇₆ nanocage. The $\Delta G_{\text{adsorption}}$ of 2Cr-C₇₆ nanocage are lower than 2Cr-Si₇₆ and 2Cr-B₃₈N₃₈ nanocages ca 0.51 and 0.25 eV. The values of $\Delta G_{\text{adsorption}}$ for Cr on Si₇₆, C₇₆ and B₃₈N₃₈ are all negative pointing out that this process is exothermic.

The formation energies ($\Delta E_{\text{formation}}$) of Si₇₆, C₇₆ and B₃₈N₃₈ nanocages and 2Cr-Si₇₆, 2Cr-C₇₆ and 2Cr-B₃₈N₃₈ are examined [29] in Table 1:

$$\Delta E_{\text{formation}} = E_{\text{nanocage}} - 76 * E_{\text{X}} \quad (4)$$

$$\Delta E_{\text{formation}} = E_{2\text{Cr-nanocage}} - E_{\text{nanocage}} - 2 * E_{\text{Cr}} \quad (5)$$

The $E_{2\text{Cr-nanocage}}$ is energies of Cr with 2Cr-Si₇₆, 2Cr-C₇₆ and 2Cr-B₃₈N₃₈, the E_{nanocage} is energies of nanocages, the E_{Cr} is energy of Cr atom and E_{X} is energies of Si, C and BN. The $\Delta E_{\text{formation}}$ of 2Cr-Si₇₆, 2Cr-C₇₆ and 2Cr-B₃₈N₃₈ nanocages are -5.25, -4.95 and -5.19 eV. The 2Cr-Si₇₆ and 2Cr-B₃₈N₃₈ nanocages have higher $\Delta E_{\text{formation}}$ than 2Cr-C₇₆ nanocage. In this study, the relative energy for acceptable spin states and spin multiplicities (S = 3, 2 and 1 and 2S+1 = 7, 5 and 3) of Cr atoms in 2Cr-Si₇₆, 2Cr-C₇₆ and 2Cr-B₃₈N₃₈ are reported in Table 2. The $\Delta E_{\text{formation}}$ of 2Cr-C₇₆ nanocage is lower than 2Cr-Si₇₆ and 2Cr-B₃₈N₃₈ nanocages ca 0.31 and 0.23 eV. The values of $\Delta E_{\text{formation}}$ of Si₇₆, C₇₆, B₃₈N₃₈, 2Cr-Si₇₆, 2Cr-C₇₆ and 2Cr-B₃₈N₃₈ are all negative. The $\Delta E_{\text{formation}}$ of Si and BN nanocages are higher than C nanocages.

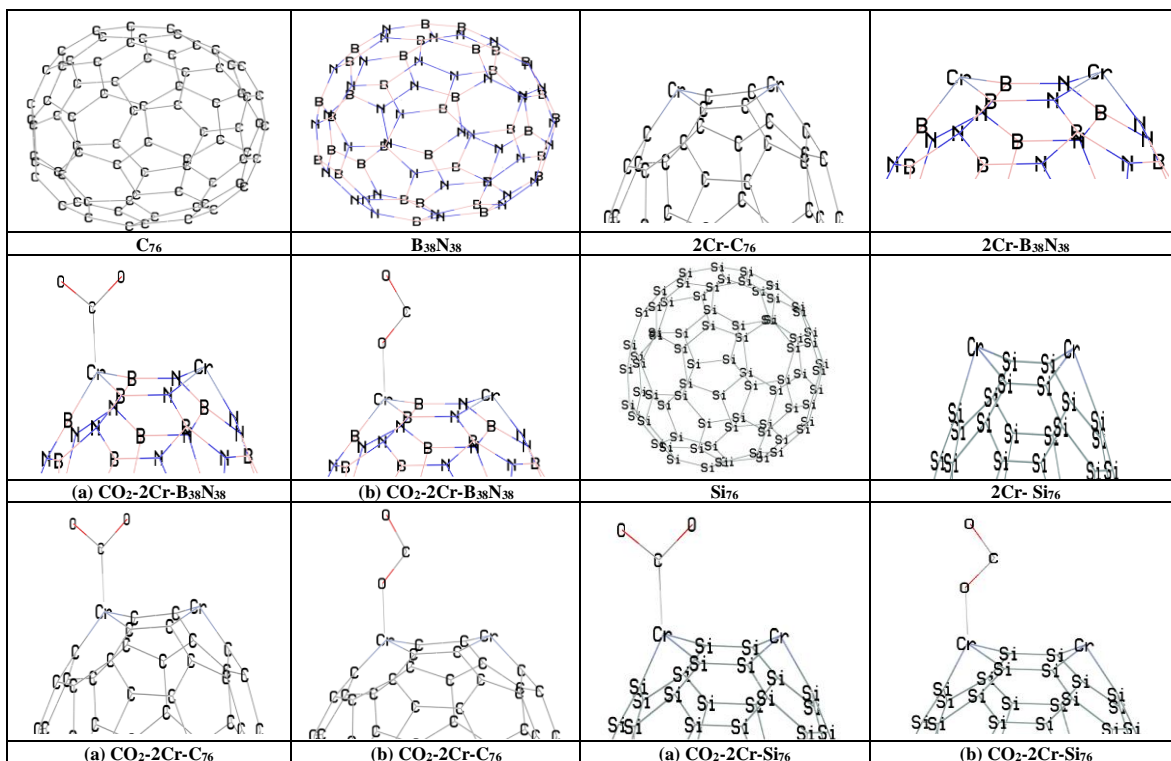


Fig. 1: Structures of Si₇₆, C₇₆ and B₃₈N₃₈ nanocages, 2Cr-Si₇₆, 2Cr-C₇₆ and 2Cr-B₃₈N₃₈ nanocages and complexes with CO₂.

Table-1: The $\Delta E_{\text{formation}}$ and $\Delta G_{\text{adsorption}}$ of 2Cr-Si₇₆, 2Cr-C₇₆ and 2Cr-B₃₈N₃₈ nanocages, the $\Delta G_{\text{adsorption}}$ of CO₂ reduction reactions on 2Cr-Si₇₆, 2Cr-C₇₆ and 2Cr-B₃₈N₃₈ nanocages.

M06-2X/6-311+G (2d, 2p)			
Nanocages	2Cr-C ₇₆	2Cr-B ₃₈ N ₃₈	2Cr-Si ₇₆
$\Delta E_{\text{formation}}$	-4.95	-4.95	-5.19
$\Delta G_{\text{adsorption}}$	-6.21	-6.21	-6.46
$\Delta G_{\text{adsorption}}$	2Cr-C ₇₆	2Cr-B ₃₈ N ₃₈	2Cr-Si ₇₆
CO ₂ (a)	-0.99	-1.07	-1.20
CO ₂ (b)	-0.90	-0.97	-1.09
CO	-2.81	-3.03	-3.41
HCOOH	-1.60	-1.73	-1.95
HCHO	-2.00	-2.16	-2.43
CH ₃ OH	-1.73	-1.86	-2.09
CH ₄	-0.85	-0.92	-1.04
PBPBE/6-311+G (2d, 2p)			
Nanocages	2Cr-C ₇₆	2Cr-B ₃₈ N ₃₈	2Cr-Si ₇₆
$\Delta E_{\text{formation}}$	-4.89	-4.86	-5.10
$\Delta G_{\text{adsorption}}$	-6.10	-6.10	-6.34
$\Delta G_{\text{adsorption}}$	2Cr-C ₇₆	2Cr-B ₃₈ N ₃₈	2Cr-Si ₇₆
CO ₂ (a)	-0.97	-1.05	-1.18
CO ₂ (b)	-0.88	-0.95	-1.07
CO	-2.76	-2.98	-3.35
HCOOH	-1.57	-1.70	-1.91
HCHO	-1.96	-2.12	-2.39
CH ₃ OH	-1.70	-1.83	-2.05
CH ₄	-0.83	-0.90	-1.02
B3LYP-D3/6-311+G (2d, 2p)			
Nanocages	2Cr-C ₇₆	2Cr-B ₃₈ N ₃₈	2Cr-Si ₇₆
$\Delta E_{\text{formation}}$	-4.92	-4.92	-5.15
$\Delta G_{\text{adsorption}}$	-6.17	-6.17	-6.41
$\Delta G_{\text{adsorption}}$	2Cr-C ₇₆	2Cr-B ₃₈ N ₃₈	2Cr-Si ₇₆
CO ₂ (a)	-0.98	-1.06	-1.18
CO ₂ (b)	-0.89	-0.96	-1.07
CO	-2.77	-2.99	-3.36
HCOOH	-1.58	-1.71	-1.92
HCHO	-1.97	-2.13	-2.40
CH ₃ OH	-1.71	-1.83	-2.06
CH ₄	-0.84	-0.91	-1.03

CO₂-RR to CO, CH₄, HCOOH, HCHO and CH₃OH on surfaces of 2Cr-Si₇₆, 2Cr-C₇₆ and 2Cr-B₃₈N₃₈ nanocages

In this section the potential of 2Cr-Si₇₆, 2Cr-C₇₆ and 2Cr-B₃₈N₃₈ nanocages to catalyze the CO₂-RR to CH₄ and CH₃OH is investigated. The three mechanisms for CO₂-RR (Pathway 1: *CO₂ → *COOH → *CO → *CHO → *CH₂O → *CH₃O → CH₃OH → *O + CH₄; Pathway 2: *CO₂ → *OCHO → *-HCOOH → *CHO → *HCHO and Pathway 3: *CO₂ → *COOH → *-HCOOH) are investigated. The adsorption of CO₂ on 2Cr-Si₇₆, 2Cr-C₇₆ and 2Cr-B₃₈N₃₈ is investigated. The structures of complexes of CO₂ on 2Cr-Si₇₆, 2Cr-C₇₆ and 2Cr-B₃₈N₃₈ nanocages are presented in Figure 1. The calculated ΔG_{adsorption} of CO₂ on 2Cr-Si₇₆, 2Cr-C₇₆ and 2Cr-B₃₈N₃₈ are summarized in Table 1.

The ΔG_{adsorption} of CO₂ on 2Cr-Si₇₆, 2Cr-C₇₆ and 2Cr-B₃₈N₃₈ nanocages via position *a* are -1.20, -0.99 and -1.07 eV. The ΔG_{adsorption} of CO₂ on 2Cr-Si₇₆, 2Cr-C₇₆ and 2Cr-B₃₈N₃₈ nanocages via position *b* are -1.09, -0.90 and -0.97 eV. The Cr atoms of 2Cr-Si₇₆, 2Cr-C₇₆ and 2Cr-B₃₈N₃₈ nanocages is adsorbed the CO₂ by O and C. The ΔG_{adsorption} of CO₂ on 2Cr-C₇₆ nanocage via positions *a* and *b* are lower than 2Cr-Si₇₆ and 2Cr-B₃₈N₃₈ nanocages ca 0.19 and 0.08 eV. The ΔG_{adsorption} of CO₂ on 2Cr-Si₇₆, 2Cr-C₇₆ and 2Cr-B₃₈N₃₈ nanocages via position *a* are higher than position *b* ca 0.09 to 0.11 eV. The 2Cr-Si₇₆ and 2Cr-B₃₈N₃₈ nanocages have higher ΔG_{adsorption} than 2Cr-C₇₆ nanocage [30-32]. The structures of CO₂-RR to create the CO, CH₄, HCOOH, HCHO and CH₃OH on 2Cr-Si₇₆, 2Cr-C₇₆ and 2Cr-B₃₈N₃₈ are presented in Figure 2. In this study, the relative energy for acceptable spin states and spin multiplicities (S = 3, 2 and 1 and 2S+1

= 7, 5 and 3) of Cr atoms in complexes of 2Cr-Si₇₆, 2Cr-C₇₆ and 2Cr-B₃₈N₃₈ with intermediates of reaction steps of CO₂-RR are reported in Table-2.

The ΔG_{reaction} and E_{barrier} of reaction steps of CO₂-RR on 2Cr-Si₇₆, 2Cr-C₇₆ and 2Cr-B₃₈N₃₈ nanocages are presented in Table 3. After adsorption of CO₂ on 2Cr-Si₇₆, 2Cr-C₇₆ and 2Cr-B₃₈N₃₈ nanocages is CO₂ protonation to create the nanocage-*COOH and nanocage-*OCHO [33, 34]. The ΔG_{reaction} of formation of nanocage-*OCHO on 2Cr-Si₇₆, 2Cr-C₇₆ and 2Cr-B₃₈N₃₈ nanocages are -0.44, -0.36 and -0.39 eV. The E_{barrier} of formation of nanocage-*OCHO on 2Cr-Si₇₆, 2Cr-C₇₆ and 2Cr-B₃₈N₃₈ nanocages are 0.23, 0.26 and 0.24 eV. The ΔG_{reaction} of formation of nanocage-*COOH on 2Cr-Si₇₆, 2Cr-C₇₆ and 2Cr-B₃₈N₃₈ nanocages are -0.35, -0.28 and -0.31 eV. The E_{barrier} of formation of nanocage-*COOH on 2Cr-Si₇₆, 2Cr-C₇₆ and 2Cr-B₃₈N₃₈ nanocages are 0.15, 0.17 and 0.16 eV.

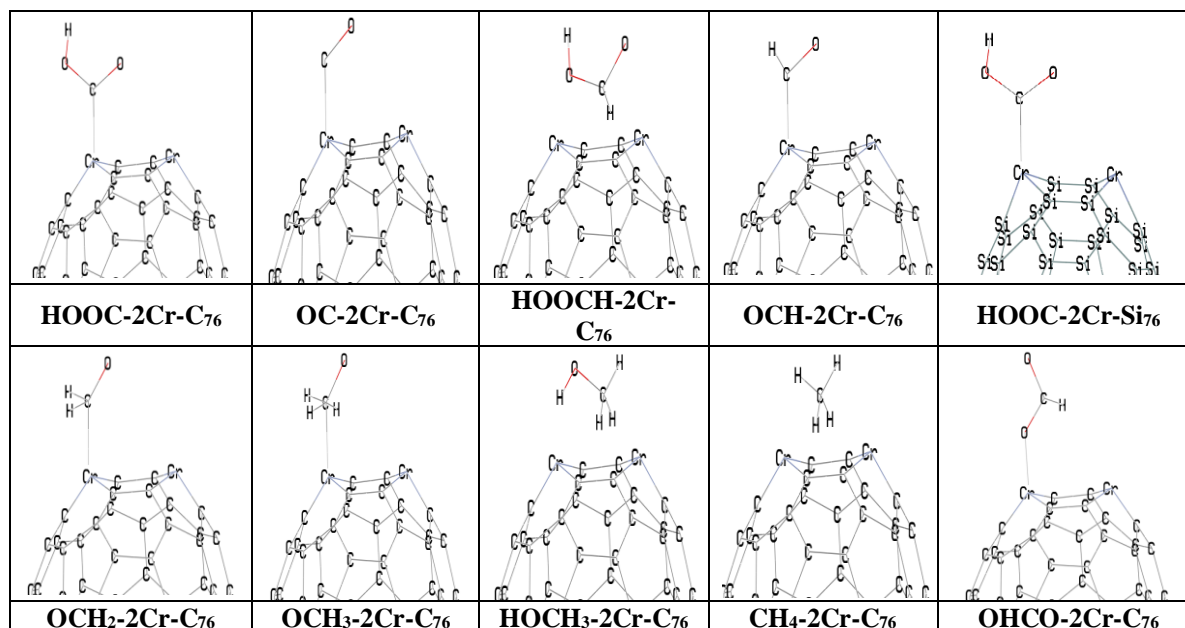
The E_{barrier} of nanocage-*OCHO is higher than nanocage-*COOH on 2Cr-Si₇₆, 2Cr-C₇₆ and 2Cr-B₃₈N₃₈ nanocages. The ΔG_{reaction} of *OCHO is more negative than *COOH on 2Cr-Si₇₆, 2Cr-C₇₆ and 2Cr-B₃₈N₃₈ nanocages and the *COOH and *OCHO are created to other possible species. The *CO is produced from *COOH on 2Cr-Si₇₆, 2Cr-C₇₆ and 2Cr-B₃₈N₃₈. The CO desorption is required high ΔG_{reaction} and CO production has low efficiency on 2Cr-Si₇₆, 2Cr-C₇₆ and 2Cr-B₃₈N₃₈. The ΔG_{reaction} of formation of nanocage-*CO on 2Cr-Si₇₆, 2Cr-C₇₆ and 2Cr-B₃₈N₃₈ nanocages are -0.37, -0.30 and -0.32 eV. The E_{barrier} of formation of nanocage-*CO on 2Cr-Si₇₆, 2Cr-C₇₆ and 2Cr-B₃₈N₃₈ nanocages are 0.23, 0.26 and 0.24 eV. The *COOH and *OCHO on 2Cr-Si₇₆, 2Cr-C₇₆ and 2Cr-B₃₈N₃₈ are converted to HCOOH.

Table-2: The relative energy in eV of 2Cr-Si₇₆, 2Cr-C₇₆ and 2Cr-B₃₈N₃₈ nanocages (S = 3, 2 and 1 and 2S+1 = 7, 5 and 3) and their complexes with intermediates of CO₂ reduction reactions.

Relative energy	2Cr-C ₇₆			2Cr-B ₃₈ N ₃₈			2Cr-Si ₇₆		
S	1	2	3	1	2	3	1	2	3
2S + 1	3	5	7	3	5	7	3	5	7
Relative energy	0.0452	0.0283	0.000	0.0416	0.0237	0.000	0.0473	0.0266	0.000
Complexes	2Cr-C ₇₆			2Cr-B ₃₈ N ₃₈			2Cr-Si ₇₆		
S	1	2	3	1	2	3	1	2	3
2S + 1	3	5	7	3	5	7	3	5	7
CO ₂ (a)	0.0450	0.0280	0.0000	0.0410	0.0230	0.0000	0.0470	0.0260	0.0000
CO ₂ (b)	0.0444	0.0276	0.0000	0.0405	0.0227	0.0000	0.0464	0.0257	0.0000
CO	0.0415	0.0258	0.0000	0.0378	0.0212	0.0000	0.0433	0.0240	0.0000
HCOOH	0.0403	0.0251	0.0000	0.0367	0.0206	0.0000	0.0421	0.0233	0.0000
HCHO	0.0389	0.0242	0.0000	0.0354	0.0199	0.0000	0.0406	0.0225	0.0000
CHO	0.0374	0.0233	0.0000	0.0341	0.0191	0.0000	0.0391	0.0216	0.0000
CH ₂ O	0.0356	0.0221	0.0000	0.0324	0.0182	0.0000	0.0371	0.0205	0.0000
CH ₃ O	0.0351	0.0218	0.0000	0.0320	0.0179	0.0000	0.0367	0.0203	0.0000
CH ₃ OH	0.0331	0.0206	0.0000	0.0302	0.0169	0.0000	0.0346	0.0191	0.0000
CH ₄	0.0305	0.0190	0.0000	0.0278	0.0156	0.0000	0.0318	0.0176	0.0000

Table-3: The $E_{\text{activation}}$, $\Delta G_{\text{reaction}}$ in eV of CO_2 -RR on 2Cr-Si₇₆, 2Cr-C₇₆ and 2Cr-B₃₈N₃₈ nanocages.

Nanocages	M06-2X/6-311+G (2d, 2p)					
	2Cr-C ₇₆		2Cr-B ₃₈ N ₃₈		2Cr-Si ₇₆	
CO ₂ reduction reaction	E _{activation}	$\Delta G_{\text{reaction}}$	E _{activation}	$\Delta G_{\text{reaction}}$	E _{activation}	$\Delta G_{\text{reaction}}$
*CO ₂ → *COOH	0.17	-0.28	0.16	-0.31	0.15	-0.35
*COOH → *CO	0.26	-0.30	0.24	-0.32	0.23	-0.37
*CO → *CHO	0.14	0.27	0.13	0.29	0.12	0.33
*CHO → *CH ₂ O	0.27	0.24	0.25	0.26	0.24	0.30
*CH ₂ O → *CH ₃ O	0.13	-0.43	0.12	-0.47	0.11	-0.53
*CH ₃ O → CH ₃ OH	0.40	-0.66	0.37	-0.71	0.35	-0.81
*CH ₃ O → *O + CH ₄	0.28	-1.38	0.26	-1.48	0.25	-1.70
*COOH → *-HCOOH	0.47	0.19	0.43	0.21	0.41	0.23
*CO ₂ → *OCHO	0.26	-0.36	0.24	-0.39	0.23	-0.44
*OCHO → *-HCOOH	0.38	-0.08	0.35	-0.09	0.33	-0.10
*HCOOH → *CHO	0.51	-0.13	0.48	-0.13	0.46	-0.16
*CHO → *HCHO	0.36	-0.64	0.34	-0.69	0.32	-0.79
PBEPBE/6-311+G (2d, 2p)						
*CO ₂ → *COOH	0.16	-0.29	0.15	-0.32	0.14	-0.36
*COOH → *CO	0.25	-0.31	0.23	-0.33	0.22	-0.38
*CO → *CHO	0.13	0.28	0.12	0.30	0.11	0.34
*CHO → *CH ₂ O	0.26	0.25	0.24	0.27	0.23	0.31
*CH ₂ O → *CH ₃ O	0.12	-0.44	0.11	-0.49	0.10	-0.55
*CH ₃ O → CH ₃ OH	0.38	-0.68	0.35	-0.73	0.33	-0.84
*CH ₃ O → *O + CH ₄	0.26	-1.43	0.25	-1.53	0.24	-1.76
*COOH → *-HCOOH	0.44	0.20	0.41	0.22	0.39	0.24
*CO ₂ → *OCHO	0.25	-0.37	0.23	-0.40	0.22	-0.46
*OCHO → *-HCOOH	0.36	-0.08	0.33	-0.09	0.31	-0.10
*HCOOH → *CHO	0.48	-0.13	0.45	-0.13	0.43	-0.17
*CHO → *HCHO	0.34	-0.66	0.32	-0.71	0.30	-0.82
B3LYP-D3/6-311+G (2d, 2p)						
*CO ₂ → *COOH	0.16	-0.29	0.15	-0.32	0.14	-0.37
*COOH → *CO	0.24	-0.31	0.22	-0.33	0.22	-0.39
*CO → *CHO	0.13	0.28	0.12	0.30	0.11	0.34
*CHO → *CH ₂ O	0.25	0.25	0.23	0.27	0.22	0.31
*CH ₂ O → *CH ₃ O	0.12	-0.45	0.11	-0.49	0.10	-0.55
*CH ₃ O → CH ₃ OH	0.37	-0.69	0.35	-0.74	0.33	-0.85
*CH ₃ O → *O + CH ₄	0.26	-1.44	0.24	-1.55	0.23	-1.78
*COOH → *-HCOOH	0.44	0.20	0.40	0.22	0.38	0.24
*CO ₂ → *OCHO	0.24	-0.38	0.22	-0.41	0.22	-0.46
*OCHO → *-HCOOH	0.36	-0.08	0.33	-0.09	0.31	-0.10
*HCOOH → *CHO	0.48	-0.14	0.45	-0.14	0.43	-0.17
*CHO → *HCHO	0.34	-0.67	0.32	-0.72	0.30	-0.83



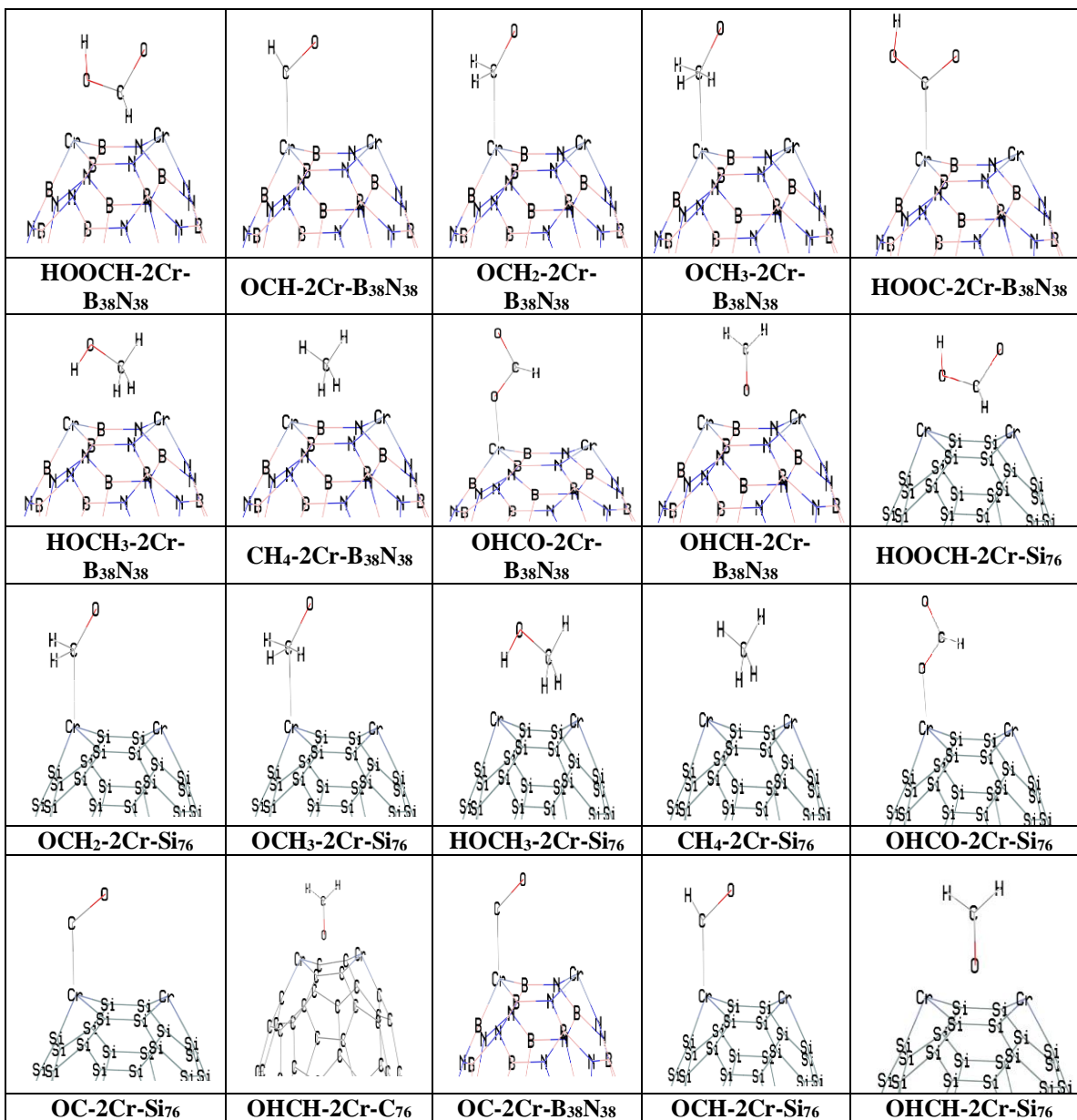


Fig. 2: Structures of complexes of CO₂-RR derivatives with 2Cr-Si₇₆, 2Cr-C₇₆ and 2Cr-B₃₈N₃₈ nanocages.

The $\Delta G_{\text{reaction}}$ values of reaction steps of CO₂-RR (Pathway 1: *CO₂ → *COOH → *CO → *CHO → *CH₂O → *CH₃O → CH₃OH → *O + CH₄; Pathway 2: *CO₂ → *OCHO → *-HCOOH → *CHO → *HCHO and Pathway 3: *CO₂ → *COOH → *-HCOOH) on 2Cr-Si₇₆, 2Cr-C₇₆ and 2Cr-B₃₈N₃₈ nanocages are presented in Figures 3, and the Gibbs free energy plan of reaction steps of CO₂-RR on 2Cr-Si₇₆, 2Cr-C₇₆ and 2Cr-B₃₈N₃₈ nanocages in various U values are presented in Figures 4. The *CO₂ → *OCHO → HCOOH reactions is favored pathway and

$\Delta G_{\text{reaction}}$ of formation of nanocage-*OCHO on 2Cr-Si₇₆, 2Cr-C₇₆ and 2Cr-B₃₈N₃₈ nanocages are -0.44, -0.36 and -0.39 eV. The E_{barrier} of formation of nanocage-*OCHO on 2Cr-Si₇₆, 2Cr-C₇₆ and 2Cr-B₃₈N₃₈ nanocages are 0.23, 0.26 and 0.24 eV. The CO and HCOOH creation on 2Cr-B₃₈N₃₈ have higher $\Delta G_{\text{reaction}}$ and lower E_{barrier} than 2Cr-Si₇₆ and 2Cr-C₇₆. The *COOH → *CO + H₂O is rate-limiting on 2Cr-Si₇₆, 2Cr-C₇₆ and 2Cr-B₃₈N₃₈ nanocages.

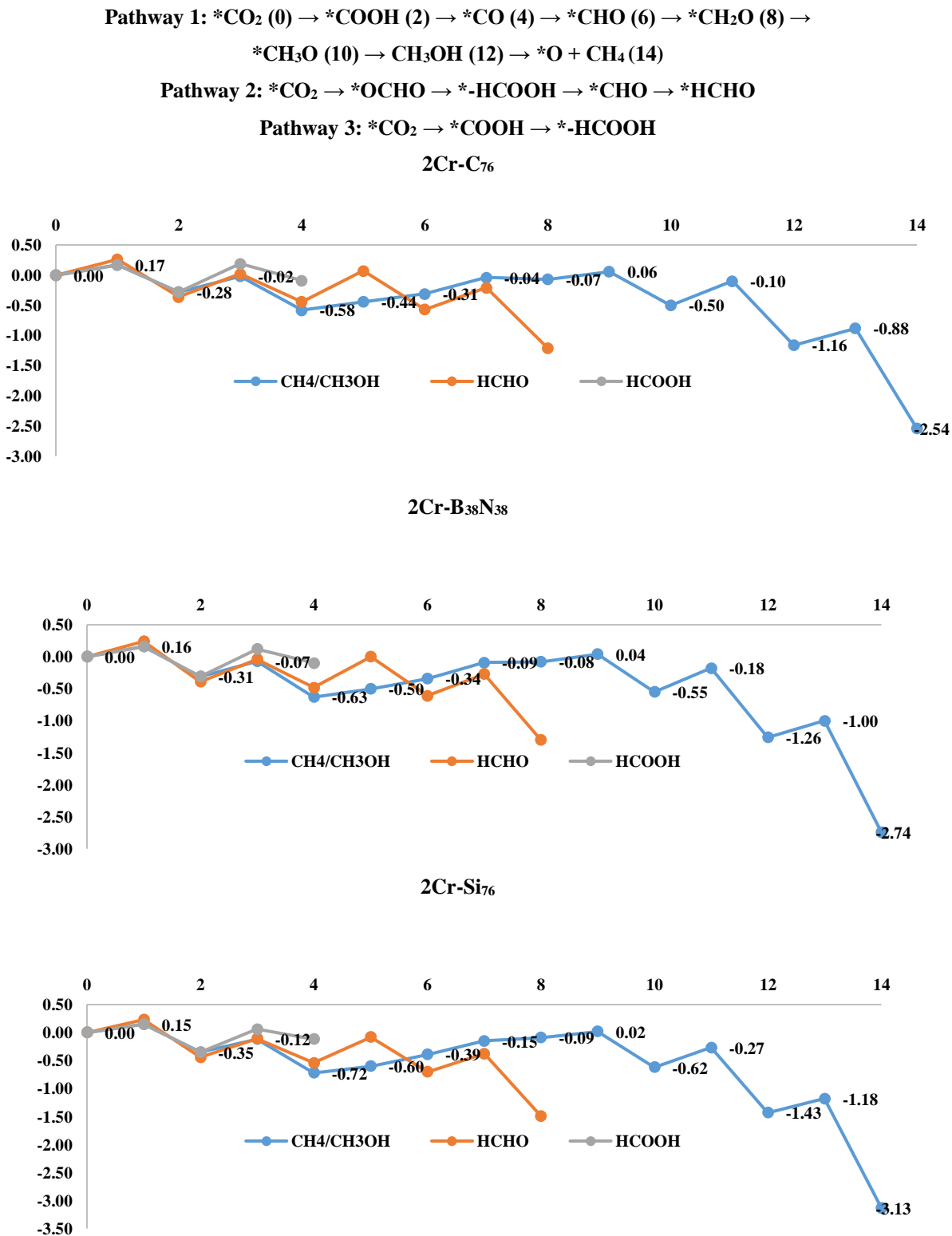


Fig. 3: The $\Delta G_{\text{reaction}}$ of reaction steps of CO_2 -RR on 2Cr-Si₇₆, 2Cr-C₇₆ and 2Cr-B₃₈N₃₈ nanocages.

The CH₃OH creation on 2Cr-Si₇₆, 2Cr-C₇₆ and 2Cr-B₃₈N₃₈ is done by acceptable pathways and *CO → *CHO is rate limiting on 2Cr-Si₇₆, 2Cr-C₇₆ and 2Cr-B₃₈N₃₈. The values of ΔG_{reaction} of CH₃OH creation on 2Cr-Si₇₆ and 2Cr-B₃₈N₃₈ nanocages are more negative than 2Cr-C₇₆ nanocage. The ΔG_{reaction} of formation of nanocage-*CH₃O on 2Cr-Si₇₆, 2Cr-C₇₆ and 2Cr-B₃₈N₃₈ nanocages are -0.53, -0.43 and -0.47 eV. The E_{barrier} of formation of nanocage-*CH₃O on 2Cr-Si₇₆, 2Cr-C₇₆ and 2Cr-B₃₈N₃₈ nanocages are 0.11, 0.13 and 0.12 eV. The reaction of CH₃OH creation on 2Cr-Si₇₆ and 2Cr-B₃₈N₃₈ nanocages have lower E_{barrier} than 2Cr-C₇₆ nanocage, significantly.

The HCHO creation on 2Cr-Si₇₆, 2Cr-C₇₆ and 2Cr-B₃₈N₃₈ nanocages is processed. The *CO → *CHO is rate-limiting of HCHO production on 2Cr-Si₇₆, 2Cr-C₇₆ and 2Cr-B₃₈N₃₈ nanocages. The ΔG_{reaction} of formation of nanocage-*CHO on 2Cr-Si₇₆, 2Cr-C₇₆ and 2Cr-B₃₈N₃₈ nanocages are 0.33, 0.27 and 0.29 eV. The E_{barrier} of formation of nanocage-*CHO on 2Cr-Si₇₆, 2Cr-C₇₆ and 2Cr-B₃₈N₃₈ nanocages are 0.12, 0.14 and 0.13 eV. The CO₂ is hydrogenated on 2Cr-Si₇₆, 2Cr-C₇₆ and 2Cr-B₃₈N₃₈ and CH₄ is created and rate limiting is the *CO → *CHO.

Results shown that the *CH₃O → CH₃OH reaction step for CO₂-RR via pathway 1 (*CO₂ → *COOH → *CO → *CHO → *CH₂O → *CH₃O → CH₃OH → *O + CH₄) on 2Cr-Si₇₆, 2Cr-C₇₆ and 2Cr-B₃₈N₃₈ is the rate-limiting step for CO₂-RR via pathway 1. The *HCOOH → *CHO reaction step for CO₂-RR via pathway 2 (*CO₂ → *OCHO → *-HCOOH → *CHO → *HCHO) on 2Cr-Si₇₆, 2Cr-C₇₆ and 2Cr-B₃₈N₃₈ is the

rate-limiting step for CO₂-RR via pathway 2. The *COOH → *-HCOOH reaction step for CO₂-RR via pathway 3 (*CO₂ → *COOH → *-HCOOH) on 2Cr-Si₇₆, 2Cr-C₇₆ and 2Cr-B₃₈N₃₈ is the rate-limiting step for CO₂-RR via pathway 3.

The over-potential for CO, HCOOH, HCHO, CH₃OH and CH₄ production via Metal-based catalysts (Fe, Ni and Co single atom as catalysts, Cu, Au, Ag based bimetallic catalysts and Pt and Pd as metal catalysts) in previous works [11-15] are summarized in Table 4. The over-potential for CO, HCOOH, HCHO, CH₃OH and CH₄ production on 2Cr-Si₇₆, 2Cr-C₇₆ and 2Cr-B₃₈N₃₈ nanocages are reported in Table 4. The over-potential for CO, HCOOH, HCHO, CH₃OH and CH₄ production on 2Cr-Si₇₆ nanocage is 0.30, 0.24, 0.27, 0.21 and 0.19 V. The over-potential for CH₄ and CH₃OH formation are lower than HCOOH on 2Cr-Si₇₆, 2Cr-C₇₆ and 2Cr-B₃₈N₃₈ nanocages. The over-potential for CO, HCOOH, HCHO, CH₃OH and CH₄ production on 2Cr-C₇₆ nanocage is 0.36, 0.30, 0.33, 0.26 and 0.24 V. The over-potential for CO, CH₄, HCOOH, HCHO and CH₃OH on 2Cr-Si₇₆ and 2Cr-B₃₈N₃₈ nanocages are lower than 2Cr-C₇₆ nanocage. The over-potential of CO₂-RR on 2Cr-C₇₆ and 2Cr-B₃₈N₃₈ are lower than Fe, Ni and Co single atom as catalysts, Cu, Au, Ag based bimetallic catalysts and Pt and Pd as metal catalysts in previous works [11-15]. The over-potential for CO, HCOOH, HCHO, CH₃OH and CH₄ production on 2Cr-B₃₈N₃₈ nanocage is 0.34, 0.27, 0.31, 0.24 and 0.22 V. The 2Cr-Si₇₆, 2Cr-C₇₆ and 2Cr-B₃₈N₃₈ are catalyzed the CO₂-RR to create the CO, CH₄, HCOOH, HCHO and CH₃OH with acceptable performance.

Table-4: The over-potential in V of CO₂-RR on 2Cr-Si₇₆, 2Cr-C₇₆ and 2Cr-B₃₈N₃₈ nanocages and reported over-potential in V of CO₂-RR on Metal-based catalysts in previous works [11-15].

M06-2X			
Overpotential	2Cr-C ₇₆	2Cr-B ₃₈ N ₃₈	2Cr-Si ₇₆
CO production	0.36	0.34	0.30
HCOOH production	0.30	0.27	0.24
HCHO production	0.33	0.31	0.27
CH ₃ OH production	0.26	0.24	0.21
CH ₄ production	0.24	0.22	0.19
PBEPBE			
Overpotential	2Cr-C ₇₆	2Cr-B ₃₈ N ₃₈	2Cr-Si ₇₆
CO production	0.34	0.32	0.28
HCOOH production	0.28	0.25	0.22
HCHO production	0.31	0.29	0.25
CH ₃ OH production	0.24	0.22	0.20
CH ₄ production	0.22	0.21	0.18
B3LYP-D3			
Overpotential	2Cr-C ₇₆	2Cr-B ₃₈ N ₃₈	2Cr-Si ₇₆
CO production	0.33	0.31	0.27
HCOOH production	0.27	0.25	0.22
HCHO production	0.30	0.28	0.25
CH ₃ OH production	0.24	0.22	0.19
CH ₄ production	0.22	0.20	0.17
Metal-based catalysts in previous works [11-15]			
Overpotential	Fe, Ni and Co single atom as catalysts	Cu, Au, Ag based bimetallic catalysts	Pt and Pd as metal catalysts
CO production	0.38	0.40	0.37
HCOOH production	0.31	0.34	0.30
HCHO production	0.35	0.37	0.34
CH ₃ OH production	0.27	0.29	0.27
CH ₄ production	0.25	0.27	0.25

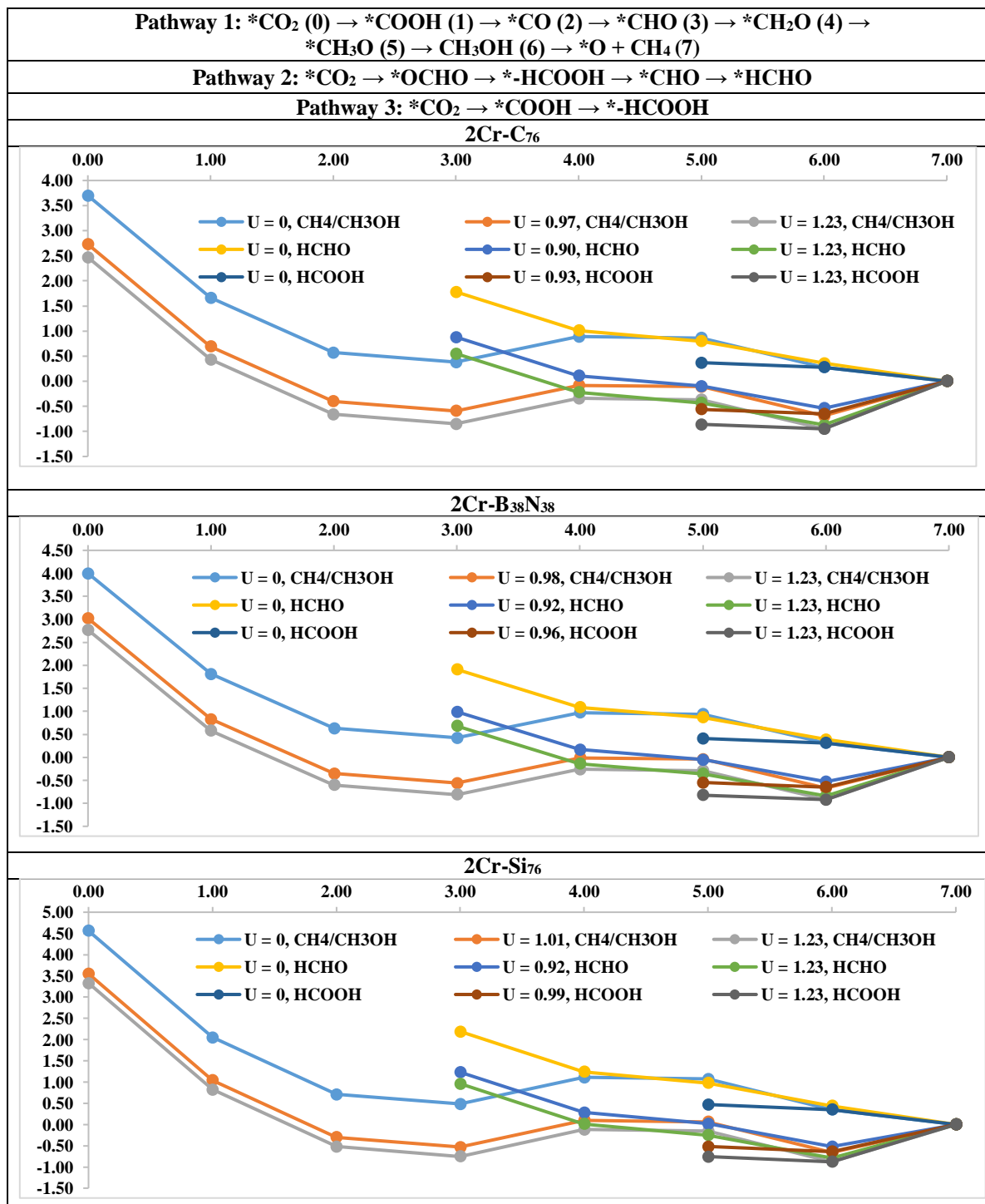


Fig. 4: The Gibbs free energy plan of reaction steps of CO₂-RR on 2Cr-Si₇₆, 2Cr-C₇₆ and 2Cr-B₃₈N₃₈ nanocages in various U values.

Conclusion

The capacities of 2Cr-Si₇₆, 2Cr-C₇₆ and 2Cr-B₃₈N₃₈ as catalysts for CO₂-RR to produce the CH₄ and CH₃OH are investigated. The $\Delta G_{\text{reaction}}$ of CO₂-RR to

create CH₄ and CH₃OH on 2Cr-Si₇₆, 2Cr-C₇₆ and 2Cr-B₃₈N₃₈ are calculated. The limiting step of creation of CH₄ and CH₃OH is *CO → *CHO on 2Cr-Si₇₆, 2Cr-C₇₆ and 2Cr-B₃₈N₃₈. The over-potential for CO, HCOOH, HCHO, CH₃OH and CH₄ production on

2Cr-B₃₈N₃₈ nanocage is 0.34, 0.27, 0.31, 0.24 and 0.22 V. The over-potential of CO₂-RR on 2Cr-C₇₆ and 2Cr-B₃₈N₃₈ are lower than Fe, Ni and Co single atom as catalysts, Cu, Au, Ag based bimetallic catalysts and Pt and Pd as metal catalysts in previous works. The 2Cr-Si₇₆ and 2Cr-B₃₈N₃₈ nanocages has higher $\Delta G_{\text{reaction}}$ and lower E_{barrier} than 2Cr-C₇₆ for CO₂-RR. The over-potential of creation of CH₄ and CH₃OH on 2Cr-Si₇₆, 2Cr-C₇₆ and 2Cr-B₃₈N₃₈ are lower than HCOOH and HCHO. Finally, the 2Cr-Si₇₆, 2Cr-C₇₆ and 2Cr-B₃₈N₃₈ are suggested as catalysts for CO₂-RR to create the CO, CH₄, HCOOH, HCHO and CH₃OH with high performance.

Acknowledgment

I thank for my university for computational support.

Ethical approval

All procedures performed in studies involving human participants were in accordance with the ethical standards of the institutional and/or national research committee and with the 1964 Helsinki declaration and its later amendments or comparable ethical standards.

References

- S. Yousaf, I. Ahmad, A. Ali. Atomically Dispersed Cu Catalysts on Sulfide-Derived Defective Ag Nanowires for Electrochemical CO₂ Reduction, *Mat. Adv.*, **5** 7891 (2024).
- M. S. Hussain, S. Ahmed, DFT Studies on a Metal Oxide@Graphene-Decorated D- π_1 - π_2 -A Novel Multi-Junction Light-Harvesting System for Efficient Dye-Sensitized Solar Cell Applications, *Nano Mat. Sci.*, **529**, 9001 (2024).
- A. Faraz, W. Iqbal, S. Gul, Selective electroreduction of CO₂ into CO over Ag and Cu decorated carbon nanoflakes, *Energy Adv.*, **3**, 2367 (2024).
- F. Chang, Z. Lin, Y. Liu, Metal-organic framework derived micro-/nano-materials: precise synthesis and clean energy applications, *Inorg. Chem. Frontiers*, **11** 5964 (2024).
- J. Yao, C. Li, K. Sun, Y. Cai, H. Li, W. Ouyang, H. Li, Ndc-scene: Boost monocular 3d semantic scene completion in normalized device coordinates space. *IEEE/CVF Int. Computer Vision* **11**, 9455 (2023).
- P. Li, J. Abbas, D. Balsalobre-Lorente, Q. Wang, Q. Zhang, S. A. R. Shah, Impact of sectoral mix on environmental sustainability: How is heterogeneity addressed? *Gondwana Res.* **128**, 86 (2024).
- J. X. Chen, L. Peng, J. Ma, H. P. Ying, Liberation of a pinned spiral wave by a rotating electric pulse. *Euro. phys. Lett.*, **107**, 38001 (2014).
- X. Sun, S. Zhu, J. Guo, S. Peng, X. Qie, Z. Yu, P. Li, exploring ways to improve China's ecological well-being amidst air pollution challenges using mixed methods. *J. Environ. Management*, **364**, 121457 (2024).
- M. Wang, W. Xu, H. Xu, H. Mu, J. Mi, Y. Wu, B. Cai, Evaluation of mechanical properties and geological features of highly sandy dolomite: consequences for engineering safety. *Bulletin Eng. Geology Environ.*, **84**, 603 (2025).
- S. Jiang, J. Zhang, K. Diao, X. Liu, Z. Ding, Research Advances in Solvent Extraction of Lithium: The Potential of Ionic Liquids. *Adv. Functional Mat.*, **11**, 2423566 (2025).
- X. Sun, Z. Meng, X. Zhang, J. Wu, The role of institutional quality in the nexus between green financing and sustainable development. *Res. Int. Business Finance*, **73**, 102531 (2025).
- M. M. Khotbehsara, M. Zadshir, B. M. Miyandehi, E. Mohseni, S. Rahmanna, S. Fathi, Rheological, mechanical and durability properties of self-compacting mortar containing nano-TiO₂ and fly ash. *J. American Sci.*, **10**, 222 (2014).
- B. Mehdizadeh, K. Vessalas, B. Ben, A. Castel, S. Deilami, H. Asadi, Advances in Characterization of Carbonation Behavior in Slag-Based Concrete Using Nanotomography. *Int. Variability*, **1**, 297 (2022).
- B. Mehdizadeh Miyandehi, K. Vessalas, A. Castel, M. Mortazavi, Investigation of Carbonation Behaviour in High-Volume GGBFS Concrete for Rigid Road Pavements. *ASCP* **1**, 12 (2023).
- A. Naseri, B. Maleki, T. Asheghi Mehmandari, A. Tohidi, A. Fahimifar, Investigating the influence of Sample geometric variations on mechanical characterization in rock and concrete. *J. Mining Environ.*, **16**, 1089 (2025).
- P. Jafari, E. Rasekh, T. Asheghi Mehmandari, M. Mohammadifar, A. Fahimifar, D. Jahed Armaghani, Upper-bound solutions for active face failure in shallow rectangular tunnels in anisotropic and non-homogeneous undrained clays. *Geotech. Geolog. Eng.*, **43**, 1 (2025).
- T. A. Mehmandari, M. Shokouhian, M. Imani, A. Fahimifar, Experimental and numerical analysis of tunnel primary support using recycled, and hybrid fiber reinforced shotcrete. *In Structures*, **63**, 106282 (2024).
- Mehmandari, T. A., Shokouhian, M., Imani, M., Tee, K. F., Fahimifar, A. Split Tensile Behavior

- of Recycled Steel Fiber-Reinforced Concrete. *ACI Mat. J.*, **122**, 5147 (2025).
19. T. A. Mehmamdar, M. Shokouhian, M. Z. Joshaghan, S. A. Mirjafari, A. Fahimifar, D. J. Armaghani, K. F. Tee, Flexural properties of fiber-reinforced concrete using hybrid recycled steel fibers and manufactured steel fibers. *J. Building Eng.*, **98**, 111069 (2024).
 20. T. A. Mehmamdar, D. Mohammadi, M. Ahmadi, M. Mohammadifar, Fracture mechanism and ductility performances of fiber reinforced shotcrete under flexural loading insights from digital image correlation (DIC). *Insight Civil Eng.*, **7**, 611 (2024).
 21. M. Ershadi, M. Javanbakht, D. Brandell, S. A. Mozaffari, A. M. Aghdam, Facile synthesis of amino-functionalized mesoporous Fe₃O₄/rGO 3D nanocomposite by diamine compounds as Li-ion battery anodes. *Appl. Sur. Sci.*, **601**, 154120 (2022).
 22. A. Molaei Aghdam, S. Habibzadeh, M. Javanbakht, M. Ershadi, M. R. Ganjali, High interspace-layer manganese selenide nanorods as a high-performance cathode for aqueous zinc-ion batteries. *ACS Appl. Energy Mat.*, **6**, 3225 (2023).
 23. A. Molaei Aghdam, N. Mikaeili Chahartagh, E. Delfani, High-Efficient Capacitive Deionization Using Amine-Functionalized ZIF-67@2D MXene: Toward Ultrahigh Desalination Performance. *Adv. Mat. Techn.*, **8**, 2300628 (2023).
 24. A. M. Aghdam, N. M. Chahartagh, S. Namvar, M. Ershadi, F. B. Ajdari, E. Delfani, Improving the performance of a SnS₂ cathode with interspace layer engineering using a Na⁺ insertion/extraction method for aqueous zinc ion batteries. *J. Mat. Chem. A*, **12**, 1047 (2024).
 25. F. B. Ajdari, F. Abbasi, A. M. Aghdam, F. G. C. Khaneh, A. G. Arjenaki, V. Farzaneh, S. Ramakrishna, Innovative self-repairing binders tackling degradation and de-lithiation challenges: Structure, mechanism, high energy and durability. *Mat. Sci. Eng. Reports*, **160**, 100830 (2024).
 26. F. B. Ajdari, P. Asghari, A. Molaei Aghdam, F. Abbasi, R. P. Rao, A. Abbasi, M. N. Chahartagh, Silicon Solid State Battery: The Solid-State Compatibility, Particle Size, and Carbon Compositing for High Energy Density. *Adv. Functional Mat.*, **34**, 2314822 (2024).
 27. N. M. Chahartagh, A. M. Aghdam, S. Namvar, M. Jafari, Enhancing the performance and cyclability of MoS₂ cathodes with interspace layer engineering using polypyrrole. *J. Mat. Chem. A*, **12**, 10875 (2024).
 28. K. Hooshyari, A. M. Aghdam, M. B. Karimi, P. Salarizadeh, M. Moradi, S. Rahmani, M. Tohidian, Lithium-Ion Batteries: Fundamental Principles, Recent Trends, Nanostructured Electrode Materials, Electrolytes, Promises, Key Scientific and Technological Challenges, and Future Directions. *Nanostruct. Mat. Energy Storage*, **1**, 31 (2024).
 29. M. N. Chahartagh, A. Molaei Aghdam, S. Namvar, F. Boorboor Ajdari, M. Ershadi, M. Jafari, Conductive Polymer Designed of Binder-Free Polypyrrole-MnO₂/Ti₃C₂ for Oxidative Stable Aqueous Zinc-Ion Batteries. *ACS Appl. Energy Mat.*, **12**, 12 (2025).
 30. A. M. Aghdam, K. Valizadeh, A. Bateni, N. Sojoodi, M. S. Jahanian, A. Kumar, J. Giao, Potential of Cu-CNT (8, 0), V-C₅₂, and Zn-SiNT (7, 0) catalysts for CO₂ reduction to CH₃OH. *J. Molec. Liq.*, **360**, 119464 (2022).
 31. F. Abbasi, F. Boorboor Ajdari, M. Mansournia, P. Asghari, A. Molaei Aghdam, Toward high energy and durable anodes: critical review on Li₄Ti₅O₁₂-MXene composites. *Carbon Lett.*, **1**, 23 (2025).
 32. Y. Ru, M. Gruninger, Y. Dou, Robust self-supervised symmetric nonnegative matrix factorization to the graph clustering. *Sci. Reports*, **15**, 7350 (2025).
 33. Y. Huo, S. Gang, C. Guan, Fcihmrt: Feature cross-layer interaction hybrid method based on Res2Net and transformer for remote sensing scene classification, *Electronics*, **12**, 4362 (2023).
 34. J. Singh, R. Abraham, Magnetic Catalyst CdFe₂O₄: Direct Conversion of Thiols into Antibacterial Sulfonamides. *Biol. Mol. Chem.*, **2**, 13 (2024).